Neuroendocrinology Letters Volume 36 No. 8 2015
ISSN: 0172-780X; ISSN-L: 0172-780X; Electronic/Online ISSN: 2354-4716
Web of Knowledge / Web of Science: Neuroendocrinol Lett
Pub Med / Medline: Neuro Endocrinol Lett

ORIGINAL ARTICLE

Brain activation sequences

Marek Susta [1,4], Hana Papezova [2], Svojmil Petranek [3], Karel Sonka [4]

1 St. Elisabeth University, Bratislava, Slovakia
2 Charles University, 1st Faculty of Medicine, Department of Psychiatry, Prague, Czech Republic
3 Bulovka Hospital, Department of Neurology, Prague, Czech Republic
4 Charles University, 1st Faculty of Medicine, Department of Neurology, Prague, Czech Republic

Correspondence to: Marek Susta
St. Elisabeth University
Nam. 1. Maja, 840 00 Bratislava, Slovakia.
e-mail: info@sciencedynamics.net

Submitted: 2015-11-02 Accepted: 2015-12-20 Published online: 2016-01-23

Key words: **qEEG; source localization; Brain Activation Sequences**

Neuroendocrinol Lett 2015; **36**(8):758–766 **PMID:** 26921576 NEL360815A03

Abstract

OBJECTIVE: Reported brain abnormalities in anatomy and function in psychiatric and neurological patients led to a project based on qualitative electroencephalography examination and analysis in an attempt to find specific brain derived pattern – or sequence of brain locations involved in processing various stimuli – both visual and auditory.
METHODS: Specialized software called Brain Activation Sequences was built according to our team member specifications (M.S.). The software utilizes event related potentials recorded during cognitive/emotion processing in participants (healthy controls, neurological patients and psychiatric patients) to calculate the sequence of brain areas using nonlinear and linear algorithms.
RESULTS: Results show significant differences in activation patterns between patients and healthy controls as well as significant similarities within the groups of patients and controls in both performed testing experiments.

INTRODUCTION

Research effort is traditionally focused on discovering differences between certain condition, disorder or illness and so called healthy controls. In some diseases the difference is so typical that all clinical implications rely, *cum grano salis*, on single gene activity and its consequences. This is the case of Huntington disease (Bastepe & Xin 2015) or ataxia telangiectasia (Nissenkorn & Ben-Zeev 2015). Although the enumeration is hardly complete, huge number of disorders and diseases remain hard to diagnose. This triggers an ongoing search for new methods capable to distinguish between certain nosological entity and healthy controls. One of the diagnostic methods with long history is electroencephalography (EEG). Despite its irreplaceable importance in epileptology, number of experts predicted the method decay after fMRI was introduced and become widely available. But the EEG equipment development has not stopped and a new generation of high density EEG machines is now used in research and clinical practice (Tucker *et al.* 2003; Kleffner-Canucci *et al.* 2012). Increase in number of electrodes from traditional 19 to 256 allows application of source localization methods and substantially lower the old disadvantage of the EEG over MRI in terms of spatial resolution (Song *et al.* 2015). The source localization accuracy is nowadays high enough to serve as pre-surgical technique minimizing need for invasive localization techniques (Yamazaki *et al.* 2012). This, together with high temporal resolution makes modern dense EEG potentially powerful diagnostic method in wide variety of applications. Our effort goes beyond the source

localization up to the field of brain connectivity in an attempt to create software tool that eases diagnostic procedures in a variety of nosologic units by discriminating between patients and healthy controls. The method, called the Brain Activation Sequences (BAS) should therefore differentiate not only particular groups, but also individuals. The method was tested on data from two independent experiments (E1) Narcolepsy with cataplexy (NC) vs. controls and (E2) Eating disorders vs. controls. Both experiments are described in scarce manner as a source of data for testing the BAS.

MATERIAL AND METHODS

Participants in the experiment 1 (E1) and experiment design

A group of 10 adult patients (5 male, 5 female) suffering from NC and 10 controls (5 male, 5 female) were examined in couple of batches. Both patients and control groups fall into similar age categories with a mean of 37 and 39 years, respectively; the difference is not significant. All patients were previously diagnosed with NC according to the International sleep disorders classification 2nd edition (American Academy of Sleep Medicine. 2005). Due to possible changes in emotion processing in NC, audio-visual humorous stimuli were selected to trigger strong positive emotions in all participants.

Participants in the experiment 2 (E2)

Ten female inpatients diagnosed with ED were selected from the Psychiatric Clinic Eating Disorders Therapy Unit. All of them have been under medication. All the patients met the criteria for ED according to DSM–IV (American Psychiatric Association 1994). Eight female healthy controls screened for any signs of eating disorder also joined the experiment. Control group exclusion criteria included also somatic diseases or psychiatric condition. Visual stimuli in this experiment included series of four faces expressing happiness, disgust, fear and surprise presented randomly for 1 second each in four batches of 50, creating 200 stimuli all together.

Both experiments were conducted in accordance with the Declaration of Helsinki and approved by the General Teaching Hospital ethical committee.

Data processing

Whole method is not entirely new. It contains procedures known and used for a long time including event related potentials and EEG-based source localization (Halliday 1980; Pfefferbaum *et al.* 1980; Grave de Peralta Menendez *et al.* 2004). The first step in obtaining BAS input data involves the EEG recording. The EEG was acquired with a 256-channel HydroCel Geodesic Sensor Net, Net Amps 300 amplifier, and Net Station, Version 4.4, software (Electrical Geodesics Inc., Eugene, OR).

All participants in both experiments (E1, E2) were fitted with a 256-channel HydroCel Geodesic Sensor Net for EEG recording and seated in front of a computer monitor. The stimulus presentation was controlled by E-Prime Software, Version 2.0 (Psychology Software Tools, Pittsburgh, PA, USA), and synchronized with EEG acquisition via the E-Prime Extension for Net Station. Stimuli were presented consecutively in the same order for each participant. Participants had approximately 1 minute to rest between trials. The total session time including EEG setup and recording lasted in both experiments (E1, E2) approximately 40 minutes.

Electrode impedances were maintained below 50 kΩ. All channels were referenced to Cz electrode during acquisition. The EEG was recorded with a 0.1-Hz to 100-Hz band-pass filter (3 dB attenuation), amplified at a gain of 1,000, sampled at a rate of 500 Hz, and digitized with a 16-bit A/D converter. The participant's facial expression in (E1) was recorded using a video-camera and microphone connected to the EEG recording computer, creating synchronized audio-video-EEG recording. During the second experiment (E2) participants were asked to sit comfortably and watch the stimulus screen.

Event-related potentials (ERPs) in experiment E1

The 256-channel HydroCel Geodesic Sensor Net covers most of a head surface including occipital region and facial muscles. After acquisition, the recording was visually inspected and all outbursts of laughter manually marked 2000 milliseconds prior to the m. zygomaticus activation (muscular artifact namely in electrodes 246 left /231 right) as a marker of laughter onset (Derks *et al.* 1997). As expected, some participants were laughing more often than others, intensity (as measured by dB) and laugh duration also varied. But the minimal number of intense laugh episodes was 7 in all participants, maximal number 16, and 11 episodes as an average.

Event-related potentials (ERPs) in experiment E2

The stimulus onset was marked automatically into the EEG recording by the experiment control machine containing E-prime software.

ERP calculation

The continuous EEG was filtered with a 30-Hz low-pass filter and 0.3 Hz high-pass filter, segmented into 2,000-ms laughter onset-locked epochs – from the emotion onset marker minus 2,000 previous milliseconds in E1 and 1000 ms with 100 ms pre-stimulus and 900 ms post-stimulus in experiment E2. Epochs contaminated with eye or movement artifact, as identified by computerized algorithm and verified by visual inspection, were eliminated, and individual bad channels were replaced on a segment-by-segment basis with spherical spline interpolation. Segments that passed all steps mentioned above without being flagged as bad, were averaged. The averaged ERPs were re-referenced to an average reference with the polar average reference effect (PARE) cor-

rection to estimate the zero surface potential integral 22 and adjusted to a 100-ms pre-emotion (E1) or pre-stimulus (E2) marker baseline. Individual ERPs were then saved in NetStation internal file format.

Source localization

The next step in calculating BAS is the source localization. There are many methods to select from – LORETA, s-LORETA or EPIFOCUS (Pascual-Marqui *et al.* 2002; Lantz *et al.* 2003). But our attention caught the fourth one. Grave de Peralta Menendez *et al.* (2001) introduced a source model constrained by the physical properties of the generators of the electrical activity. The first model developed by Grave de Peralta Menendez was called the ELECTRA and worked quite well, but the solution provided was non-unique. The strategy of a unique solution selection named LAURA (Local Autoregressive Average) utilizes several techniques based on the following statements. EEG measurement is not capable to determine all brain locations activity. The electrical activity at each point can be to some extent expressed as a combination of the information recorded *in situ* and the local neighbors. Newtonian potential is a function of the inverse of the distance and electric potential decays as a function of the square distance while electric field decays with the third power of the inverse distance. The activity at each site is then expressed as a function of the neighbors using a local autoregressive estimator (Ripley 1981) based on coefficients dependent on the distance to the target point (Equation 1):

$$f_i = \frac{N_i}{N} \sum_{k \subset V_i} \frac{d_{ki}^{-e_i}}{\sum_{k \subset V_i} d_{ki}^{-e_i}} f_k$$

The equation described in detail by Gonzales (1999) calculates the function value as a weighted sum of the unknown neighboring function values. The f value describes consistent local average. N_{max} for the 3-D space is 26, N_i is actual number of neighbors. The area is then defined by a hexahedron with the center at i. The exponent e_i takes value from 1 to 3 to express the distance differences. The N_i/N fraction corrects the constant function estimation, because there are no primary sources outside the brain. The next step in the LAURA method is expressed by (Equation 2):

$$g_i = w_i \left\{ \frac{N}{N_i} \left[\sum_{k \subset V_i} d_{ki}^{-e_i} \right] f_i - \sum_{k \subset V_i} d_{ki}^{-e_i} \; f_k \right\}$$

where the norm of the field g is minimized with components less dependent than in the previous equation. One element g near zero implies that the corresponding element of f is substantially predicted by its neighbors and not by the recording site itself. The discrete version of the inversion problem (Equation 3):

$$d = L * J + n$$

where d expresses data measured on n sensors, J is the discretization of the unknown function on np solution points and vector n represents additive noise. The solution is then obtained by solving the following equation for Np vector J (Equation 4).

$$d - LJ + \lambda * R(J)$$

where regularization operator is (Equation 5):

$$R(J) = WAJ$$

From equation 2, the diagonal element of the *i-th* row of A is (Equation 6):

$$A_{ii} = \frac{N}{Ni} \sum_{k \subset V_i} d_{ki}^{-e_i}$$

where V_i stands for the vicinity of the *i-th* solution point and d_{ki} is the distance from the *k-th* neighbor to the target point *i*. The off-diagonal elements are equal to zero with the exception of $k \subset Vi$ where it equals to (Equation 7):

$$A_{ik} = -d_{ki}^{-e_i}$$

The e_i value was set to 2 for all calculations. For the estimation of the current density vector the regularization operator is calculated by (Equation 8):

$$R(J) = (WA \otimes I_3)J$$

where $\otimes$ represents the Kronecker product of matrices (Rao & Mitra 1971)and the elements of the diagonal matrix W are selected as the mean of the 3 columns of the lead field matrix associated with *i*. This weighting approach significantly increases localization capabilities of the LAURA method. The LAURA method was applied to data obtained in ERP step of the analysis. There are multiple options in inverse solution settings. The first decision to make is sparse versus dense dipole set. Sparse dipole set contains 57 dipoles that are distributed across the functional regions of the cerebral cortex. On the other hand, dense dipole set contains 2,447 dipoles that are distributed in 7 mm voxels across the cortex, with each dipole being represented by a triple regional source in the orthogonal orientations. Due to computational power of the equipment and quality of input data obtained from 256 surface locations, the dense dipole set was used for calculation. Precise calculation requires as less generalization and assumptions as possible. Individual MRI recordings were used to confirm inverse solution accuracy in comparison with generalized finite difference model (Vanrumste *et al.* 2001), based on analysis of the geometry and conductivity of the tissues of a typical head using detailed MRIs and CTs. There were no significant differences between individual/general head model given the fact that localization accuracy is mainly given by a number of surface sites. As confirmed by a recently published experiment, the most accurate source localization is obtained when the voltage surface is densely sampled over both the superior and inferior surfaces (Song *et al.* 2015). Final selection is the design of the

output. It could generally be one of the following: all dipoles (AD), sparse matrix (SM), Brodmann areas (BA) and selected gyri-like locations (G). Going back to our original question of finding a pattern discriminating between laughter processing in narcolepsy and in healthy subjects, the simplest but still effective output will suffice. Data was then exported in delimited text format covering activity in respective area based on selected output type (columns) over time times sampling frequency (rows).

Brain Activation Sequences

Large number of options, given by the extensive input data, wide variety of analytic methods and need for unified output capable of answering our original question clearly required specialized software solution created just for the task. Our search for specific pattern, distinguishing between certain groups of subjects inspired development of the software we call "Brain Activation Sequences" (BAS). This software allows user to import subject EEG data and run selected analysis. The analysis output, in a form of a sequence of brain areas, is then displayed and stored. All inverse problem outputs described in the previous paragraph were tested during BAS software development and calibration. When all dipoles are selected (AD), number of columns of the input file gets up to 2447 and covers therefore all calculated voxels one by one. Although most exact, this method consumes most computational resources meaning a 72 times longer computation duration compared to the one finally selected for BAS, as well as delivering output that is too detailed. Our search for patterns would require grouping of voxels into clusters anyway. The second output option, sparse matrix (SM) gives activity in 57 preselected general cortical locations. This method fits our plans much better than the previous one, but these pre-selected locations include mostly surface cortical areas and our interest is in both cortical and subcortical brain areas. The third output option BA, fits our plans in terms of grouping, but also focuses on the surface. This leads us to the last (G) method of selected gyri-like locations. The brain is divided into 66 areas (Yamazaki *et al.* 2013), usually identical with gyri of both brain hemispheres (left and right) but not in all cases. Some area names and definition correspond to the division in Talairach coordinates used mainly in radiology (Bankman 2000). Brain areas of our interest are covered from lateral and medial perspective thus matching our requirements – the method of gyri-like locations (G) activity matrix over time had been selected as a data source for the final step in analysis. All previously described steps and calculations can be performed by standard issue software and/or publicly available sources. The algorithm had been developed by one

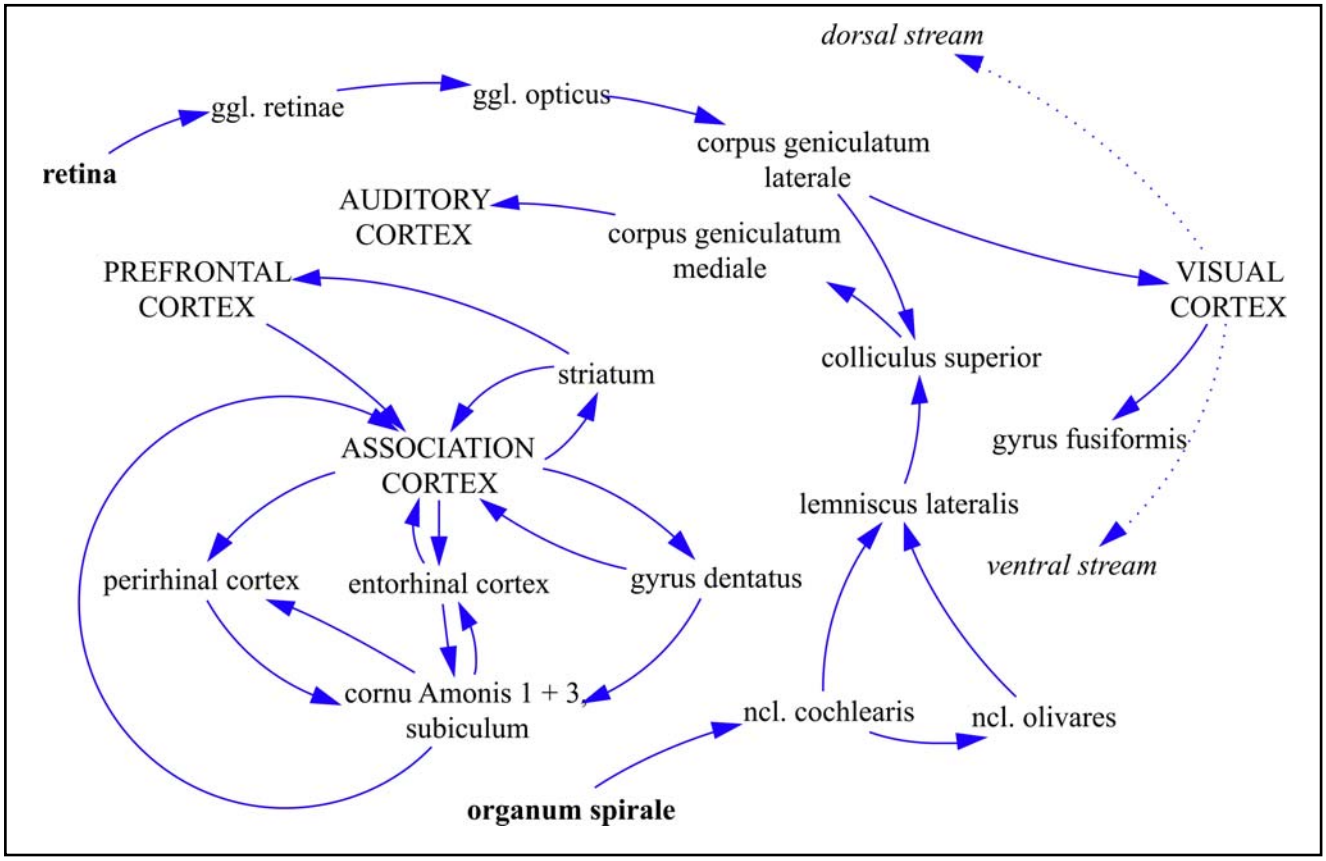

Fig. 1. Partial diagram of visual, memory and auditory pathways used as a mental base for computer model.

of us (M.S.). Proverbs Corporation (Zitna 52, Prague, Czech Republic) created, according to our specification, specialized BAS software to ensure calculations accuracy, increase user comfort and minimize errors.

Once the trial data in a format explained in previous paragraphs are loaded into the BAS, the process starts with a nonlinear model application. The nonlinear model is a large set of feedback-driven differential equations, which form a dynamic structure capable to simulate selected brain processes. The structure is dynamically weighting input from the trial and calculating dominant structure for each time step based on System Dynamics approach as defined by Forrester (Forrester 1975). The system dynamics approach has been used to simulate selected brain-related processes connected to traumatic stress (Bizik & Susta 2012; Susta & Bizik 2012), but BAS is using generalized pathways structure, partly denoted in Figure 1.

Both experiments (E1, E2) utilize visual, memory and emotion pathways, in addition, experiment E1 also uses auditory pathway.

The visual pathway originates from the retina and goes to the primary visual cortex via the thalamic lateral geniculate nucleus. From the visual cortex the information reaches extrastriate cortex along the occipitotemporal (Ventral) and occipitoparietal (Dorsal) stream. Another fibers originating from the same source follow the route into superior colliculus and pulvinar. From these two sites the signal goes directly into the exstrastriate cortex, bypassing the primary visual cortex. The third pathway, independent from primary visual cortex is formed by direct projections between the superior colliculus and lateral geniculate nucleus sending efferents to extrastriate cortices of the dorsal stream (Tamietto & de Gelder 2010). We therefore expect to find some of these structures involved especially in both (E1, E2) experiments. We are also getting emotional response from participants. Emotional pathways include connections between amygdala, substantia innominata, nucleus acumbens and brainstem nuclei locus coeruleus and periaqueductal grey. Another connections lead from amygdala to anterior cingulate cortex and orbitofrontal cortex. Especially subcortical structures of visual and emotional systems are considerably interconnected; the pathway goes from superior colliculus through pulvinar into amygdala and nucleus accumbens. We have been describing so far systems involved in so called non-conscious perception and we did it on purpose. Only a fraction of sensory input activates conscious perception. Filtering out what is relevant for conscious perception is called selective attention (Posner 1994; Posner & Dehaene 1994). Evidence shows that visual stimuli that lie outside focus of attention are attenuated or abolished (Mack & Rock 1998). When there is a task with attention resources involved, cortical activity evoked by task-irrelevant stimuli is suppressed by fronto-parietal areas (Beck *et al.* 2001). But there is one important exception – emotional stimuli. With emotions involved, the stimulus gets the highest priority (Takahashi 2013). It does not mean that all stimuli packed with emotions will stop or reroute task at hand, but even "ignored" emotional stimuli interfere with processed information, delay disengagement of attention and are generally easier to detect (Ohman *et al.* 2001). Not all structures, namely subcortical ones, mentioned above are reachable by the qEEG inverse solution. But our focus was on accessible ones. Spatial resolution used in visual, memory, emotion and auditory pathways description above roughly fits the resolution required for BAS calculation. Knowing what general task is being processed (purely visual, purely auditory, audio-visual, auditory-emotional etc.) the model simulates expected and real activation of selected areas. Output from the LAURA in a form of matrix with x-axis representing time steps (Equation 9):

$$S = L * f_s$$

where S is the number of time steps, L is the length of the ERP segment in seconds and f_s represents EEG recording sampling frequency. The y-axis of the matrix then contains activity in selected locations, described above with values in nAm (nano Amper-meters). The subjects database in BAS software contains experiment type data and basic clinical information on subject (age, sex, preliminary diagnosis). With the exception of experiment data, no parameters are used for further processing. That is, the algorithm is "unaware" of the diagnosis, age or any other parameters that might affect the output. The matrix in plain text format is then imported into BAS software with patient number and experiment code header.

The BAS software user can immediately access algorithm selection radio buttons and therefore choose data processing mode. Algorithms I and II and III actually bypass nonlinear simulation model and calculate the output using simple statistics of selecting the location with maximal activity in given time-step t_s that differs from maximum in t_{s-1} (Algorithm I), maximal activity location in given time-step t_s that was not selected so far in $<t_0, t_{s-1}>$ (Algorithm II), or simple maximal activity location over the whole time-span $<t_0,t_{smax}>$ even if the algorithm marks only one brain location as most active (Algorithm III). Algorithms IV–VII use nonlinear differential model structure to calculate final output sequence. The input matrix enters the structure through selected model parameters (Insular Sin, Fusiformis Dx etc. in Figure 2) forming the baseline that is continuously compared with simulated activity based on experiment type. The figure shows model structure processing facial expression stimulus. Note the time graphs – although the pattern is not the same, the dynamics is similar enough, with overall fit at the end of simulation 86.17% (Figure 3). Simulation structure cannot fit the real pattern entirely, because of other tasks processed by the same structures in reality influencing final gyral dynamics. The model calculates real-

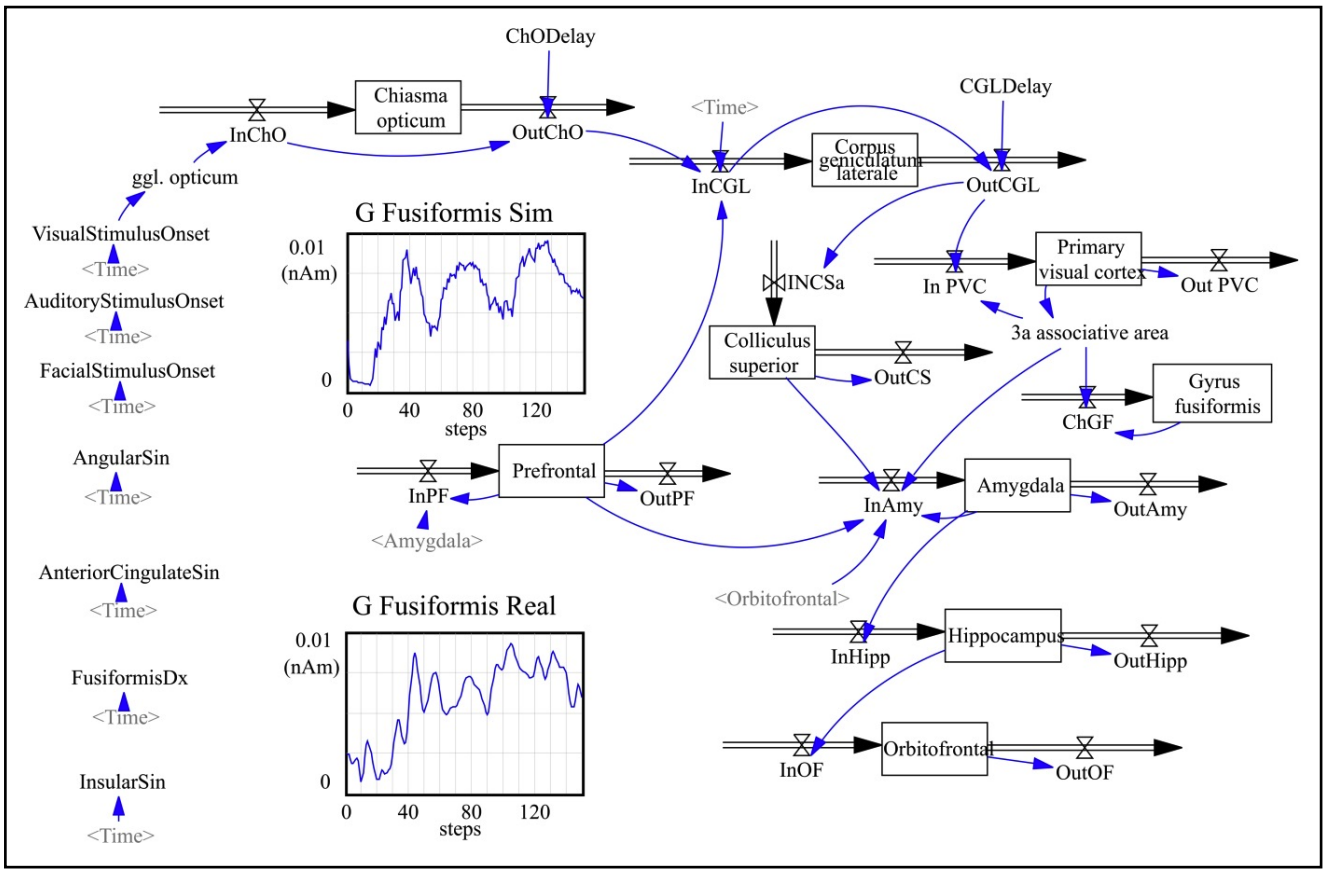

Fig. 2. Partial brain model structure. G-Fusiformis Sim – simulated activity of gyrus fusiformis in reaction to facial expression stimulus. G-Fusiformis Real – real pattern of gyrus fusiformis activity in subject C2. All (In…) variables refer to the inflow into the state variable (e.g. Chiasma opticum, Prefrontal) that accumulate inflow and are depleted by the outlow (Out…). Variables like ChODelay (Chiasma opticum delay) represent delays between inflow and outflow in particular structure.

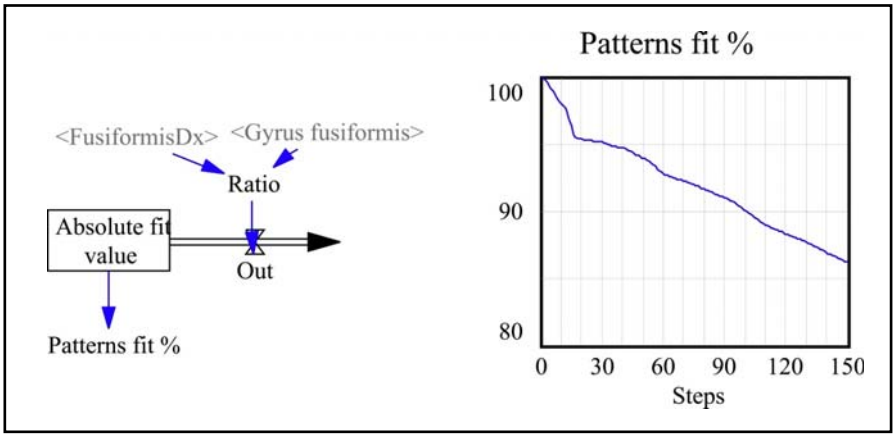

Fig. 3. Patterns fit calculation with model structure (left) and time-graph (right). The accuracy sharply drops at the beginning of simulation and then follows less steep decay with 86% of accuracy over the 150 steps.

ity/simulation ratio in all activated gyri and gyri-like locations and by modifying the influence of the most active gyrus or delaying location dominance impact calculates the output matrix that enters final processing. The simulated pattern influence is a time-dependent. That means the difference in patterns is not the ultimate reason for any action unless it crosses time-dependent tipping point. The tipping point x-axis location is given by the level of experiment "noise" that differs substantially among experiment type. Single audio tone with eyes closed is accompanied by less supplemental brain activity than watching a movie with strong emotional content (Pallesen *et al.* 2009; Youssofzadeh *et al.* 2015).

The final calculation in model IV, V, VI and VII is built as a recursive algorithm resulting in table with a sequence of brain locations in descendent order till the end of sequence. The nonlinear model settings are applied to all trial participants – patients and healthy controls. Software does not take into account group membership (whether the patient or healthy control is processed), but calculates sequence for every subject and saves it into an internal database table.

RESULTS

There are more means of displaying results in BAS software. Two examples of individual results are in Figure 4. The figure shows different activation patterns in typical control subject (left side screen shot) and typical patient (right side of the screen) (Experiment E1) calculated using so-called algorithm V, a recursive algorithm working with cumulative outputs of the non-linear structure mentioned in previous paragraphs. The first twelve output steps, which form the BAS are shown in all four print screens. The differences and similarities between patients and controls are clear at first sight but detailed comparison of active gyri in both groups are in Table 1.

Healthy controls follow the pattern involving orbito-temporo-occipital route, while patients descend along the fronto-medio-temporo-occipital path. This does not mean that other brain areas are not involved, but those displayed significantly contribute, according to the EEG recording and the BAS post-processing. Selected brain areas, mostly gyri were imported from the BAS software output table and processed statistically. Results in Table 1 show the presence of locations in activation sequences in patient and healthy participant groups. The first four locations are present in all patient sequences and none are present in the healthy controls. This applies to recursive algorithm that utilizes all cumulative data results from BAS software non-linear dynamic structure.

Results of the Experiment 2 (E2) is in Figure 5 where the difference between healthy controls (left) and patients (right) is again clearly notable. Healthy controls follow the orbitalis-angularis-occipitalis route, while patients completely skip the angularis and activate uncus instead. Sumarized information on activated locations is in Table 2.

Tab. 1. Brain locations and their presence in BAS based on full data table, audio-visual (AV) stimulation during the E1 experiment.

Location (gyrus)	Presence in:	
	Patients (N=10)	Healthy Controls (N=10)
paracentralis	100%	0%
cinguli	100%	0%
cingularis posterior	100%	0%
cuneus dx	100%	0%
uncus	50%	40%
frontalis medialis	90%	0%
occipitalis inferior	80%	30%
orbitalis	0%	90%
rectus	0%	100%
extra-nuclear (TALg)	0%	90%
subralossal	0%	70%
temporalis transversus	20%	90%

Tab. 2. Brain locations and their presence in BAS based on full data table, emotion face stimulus in E2 experiment.

Location (gyrus)	Presence in:	
	Patients (N=10)	Healthy Controls (N=8)
orbitalis	100%	100%
rectus	100%	100%
uncus	100%	0%
occipitalis superior	60%	63%
extra-nuclear (TALG)	40%	0%
cuneus	50%	0%
temporalis inferior	20%	0%
angularis	0%	100%
temporalis transversus	0%	100%
occipitalis inferior	0%	100%

DISCUSSION

The whole idea of connectivity of certain brain areas and functional difference between NC and patients is based on research findings in fMRI and anatomic studies. We have tried to identify these differences using our own method called BAS. According to our original expectations, the BAS should discriminate between both above mentioned groups with (preferably) high accuracy. It seems to be clear that this software tool works only in cases where stimulus processing differs in patients and controls. Crucial part of the application is in obtaining valid ERP source data with respect to patient condition and medication (Sonka *et al.* 2014). In our experiment E1, pre-laughter segments were used to calculate input data, laughing subject is therefore condition *sine qua non*. In cases where subjects are less cooperative, for example due to psychiatric condition, experiment design must reflect the reality and experiment should not require long attention times or any form of manual reaction (e.g. pressing the button etc.) that subject perceive as a burden. This approach on the other hand means that ERPs could not be in all cases as clearly different between patients and controls as experiment designer expects but maintaining a balance is a part of researcher's job. Differences in BAS between controls and patient groups and similarities within these groups are in both experiments clear (Figures 4 and 5, Tables 1 and 2). Although selected method of source localization does not reach fMRI spatial accuracy, temporal resolution of the high-density EEG combined with advanced analytic methods provide enough data to find patterns clearly discriminating between

Fig. 4. Brain Activation Sequences in Experiment 1 (E1) – pattern for healthy controls (left), patterns for NC (right), audio-visual stimulation. Areas in pink color refer to the medial view, areas in violet cover lateral view.

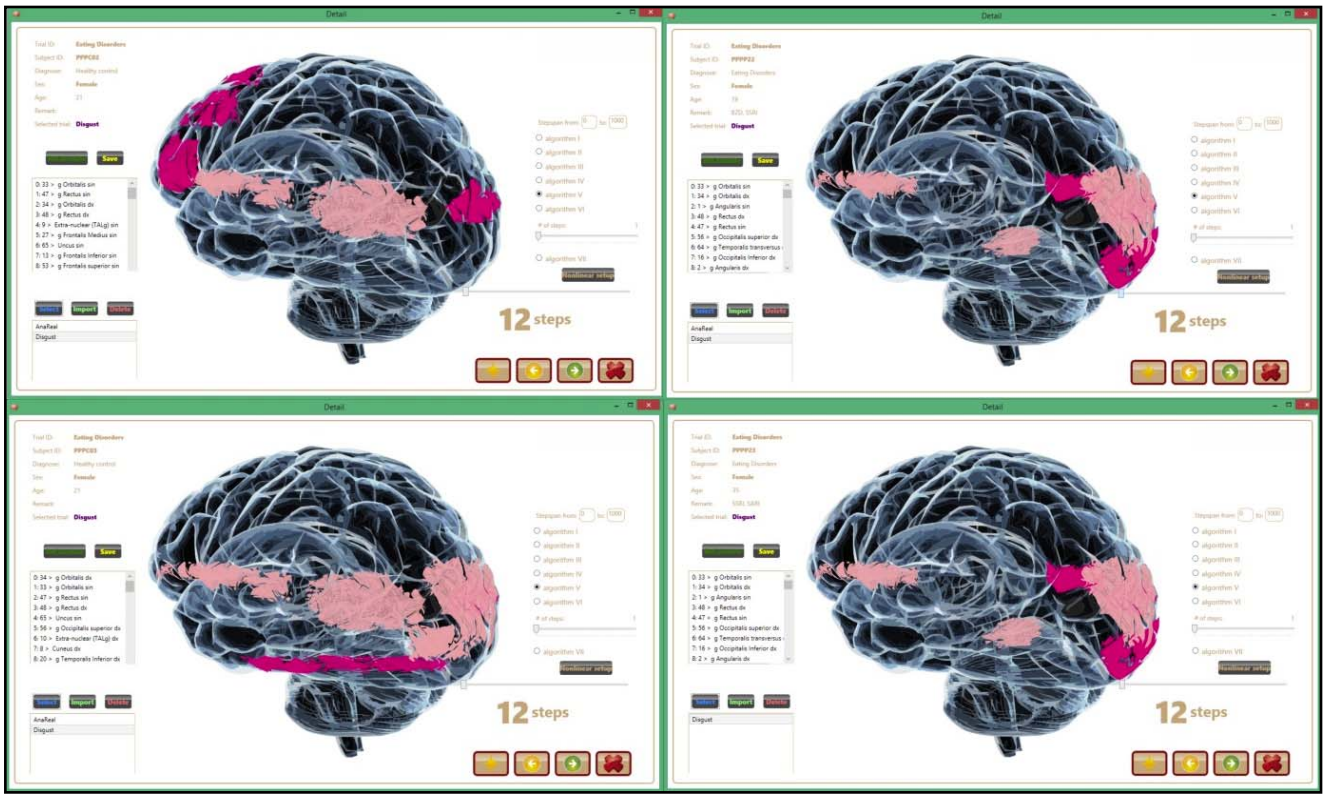

Fig. 5. Brain Activation Sequences in Experiment 2 (E2) – pattern for healthy controls (left), patterns for eating disorders (right), stimulated by emotion face expressing disgust. Areas in pink color refer to the medial view, areas in violet cover lateral view.

both study groups. There are questions that still need to be answered and a less complicated study design or equipment might be sufficient as an input data source for BAS algorithm, however, we think that that BAS is a promising method to study brain activity within different tasks in healthy state and in brain disorders. One can speculate that BAS will in future not only answer pathophysiology process in various brain diseases but might also serve as a diagnostic tool.

ACKNOWLEDGEMENTS

This research project had been supported by the Czech Ministry of Health grant NT13238-4/2012, Charles University grant PRVOUK P26/LF1/4 and Proverbs 2012-5/3/02 grant.

REFERENCES

1 American Academy of Sleep Medicine. (2005). The international classification of sleep disorders: diagnostic and coding manual. Westchester, Ill.: American Academy of Sleep Medicine.
2 Bankman IN (2000). Handbook of medical imaging : processing and analysis. San Diego, CA: Academic Press.
3 Bastepe M, Xin W (2015). Huntington Disease: Molecular Diagnostics Approach. Curr Protoc Hum Genet **87**: 9 26 1–9 26 23.
4 Beck DM, Rees G, Frith CD, Lavie N (2001). Neural correlates of change detection and change blindness. Nat Neurosci **4**: 645–50.
5 Bizik G, Susta M (2012). Cortisol dynamics in traumatised, PTSD and PTSD+MDD patients. Biogenic Amines **26**: 101–113.
6 Derks P, Gillikin LS, Bartolome-Rull DS, Bogart EH (1997). Laughter and electroencephalographic activity. Humor – International Journal of Humor Research **10**: 285–300.
7 Forrester JW (1975). Collected papers of Jay W. Forrester. Cambridge, Mass.: Wright-Allen Press.
8 Grave de Peralta Menendez R, Gonzalez Andino S, Lantz G, Michel CM, Landis T (2001). Noninvasive localization of electromagnetic epileptic activity. I. Method descriptions and simulations. Brain Topogr **14**: 131–7.
9 Grave de Peralta Menendez R, Murray MM, Michel CM, Martuzzi R, Gonzalez Andino SL (2004). Electrical neuroimaging based on biophysical constraints. Neuroimage **21**: 527–39.
10 Halliday AM (1980). Event-related potentials and their diagnostic usefulness. Prog Brain Res **54**: 469–85.
11 Kleffner-Canucci K, Luu P, Naleway J, Tucker DM (2012). A novel hydrogel electrolyte extender for rapid application of EEG sensors and extended recordings. J Neurosci Methods **206**: 83–7.
12 Lantz G, Grave de Peralta R, Spinelli L, Seeck M, Michel CM (2003). Epileptic source localization with high density EEG: how many electrodes are needed? Clin Neurophysiol **114**: 63–9.
13 Mack A, Rock I (1998). Inattentional blindness. Cambridge, Mass.; London: MIT Press.
14 Nissenkorn A, Ben-Zeev B (2015). Ataxia telangiectasia. Handb Clin Neurol **132**: 199–214.
15 Ohman A, Flykt A, Esteves F (2001). Emotion drives attention: detecting the snake in the grass. J Exp Psychol Gen **130**: 466–78.
16 Pallesen KJ, Brattico E, Bailey CJ, Korvenoja A, Gjedde A (2009). Cognitive and emotional modulation of brain default operation. J Cogn Neurosci **21**: 1065–80.
17 Pascual-Marqui RD, Esslen M, Kochi K, Lehmann D (2002). Functional imaging with low-resolution brain electromagnetic tomography (LORETA): a review. Methods Find Exp Clin Pharmacol **24**(Suppl C): 91–5.
18 Pfefferbaum A, Ford JM, Roth WT, Kopell BS (1980). Age-related changes in auditory event-related potentials. Electroencephalogr Clin Neurophysiol **49**: 266–76.
19 Posner MI (1994). Attention: the mechanisms of consciousness. Proc Natl Acad Sci U S A **91**: 7398–403.
20 Posner MI, Dehaene S (1994). Attentional networks. Trends Neurosci **17**: 75–9.
21 Rao CR, Mitra SK (1971). Generalized inverse of matrices and its applications. New York,: Wiley.
22 Ripley BD (1981). Spatial statistics. New York ; Chichester: Wiley.
23 Song J, Davey C, Poulsen C, Luu P, Turovets S, Anderson E, *et al.* (2015). EEG source localization: Sensor density and head surface coverage. J Neurosci Methods **256**: 9–21.
24 Sonka K, Sos P, Susta M (2014). Past and present in drug treatment of sleep disorders. Neuro Endocrinol Lett **35**: 186–97.
25 Susta M, Bizik G (2012). Human stress response from the system dynamics point of view. Biogenic Amines **26**: 30–41.
26 Takahashi T (2013). A psychophysical theory of Shannon entropy. Neuro Endocrinol Lett **34**: 615–7.
27 Tamietto M, de Gelder B (2010). Neural bases of the non-conscious perception of emotional signals. Nat Rev Neurosci **11**: 697–709.
28 Tucker DM, Luu P, Frishkoff G, Quiring J, Poulsen C (2003). Frontolimbic response to negative feedback in clinical depression. J Abnorm Psychol **112**: 667–78.
29 Vanrumste B, Van Hoey G, Van de Walle R, D'Have MR, Lemahieu IA, Boon PA (2001). The validation of the finite difference method and reciprocity for solving the inverse problem in EEG dipole source analysis. Brain Topogr **14**: 83–92.
30 Yamazaki M, Tucker DM, Fujimoto A, Yamazoe T, Okanishi T, Yokota T, *et al.* (2012). Comparison of dense array EEG with simultaneous intracranial EEG for interictal spike detection and localization. Epilepsy Res **98**: 166–73.
31 Yamazaki M, Tucker DM, Terrill M, Fujimoto A, Yamamoto T (2013). Dense array EEG source estimation in neocortical epilepsy. Front Neurol **4**: 42.
32 Youssofzadeh V, Prasad G, Fagan AJ, Reilly RB, Martens S, Meaney JF, *et al.* (2015). Signal Propagation in the Human Visual Pathways: An Effective Connectivity Analysis. J Neurosci **35**: 13501–10.